Supplementary Material (ESI) for Chemical Communications
This journal is (c) The Royal Society of Chemistry 2011

Novel cerium-tungsten mixed oxide catalyst for the selective catalytic reduction of NO_x with NH_3

Wenpo Shan, Fudong Liu*, Hong He, Xiaoyan Shi, Changbin Zhang

State Key Laboratory of Environmental Chemistry and Ecotoxicology, Research Center for Eco-Environmental Sciences, Chinese Academy of Sciences, Beijing 100085, China

*Corresponding author. Tel: 86-10-62911040; Fax: 86-10-62911040;
E-mail address: fdliu@rcees.ac.cn

Electronic Supplementary Information

Preparation of $Ce_aW_bO_x$, V_2O_5-WO_3/TiO_2 and Fe-ZSM-5 catalysts

The serial Ce-W mixed oxide catalysts were prepared by homogeneous precipitation method using cerium nitrate and ammonium tungstate as precursors. $(NH_4)_{10}W_{12}O_{41}$ with equal weight $H_2C_2O_4 \cdot 2H_2O$ were added to deionized water. After the dissolution of $(NH_4)_{10}W_{12}O_{41}$, the aqueous solution of $Ce(NO_3)_3 \cdot 6H_2O$ was added with required molar ratio (Ce/W = 2:1, 1:1 and 1:2). Excessive urea aqueous solution was then added into the mixed solution, with an urea/(Ce + W) molar ratio being 10:1. The mixed solution was then heated to 90 ºC and held there for 12 h under vigorous stir. After filtration and washing with deionized water, the resulting precipitant was dried at 100 ºC overnight and subsequently calcined at 500 ºC for 5 h in air condition. The obtained catalysts were denoted as $Ce_aW_bO_x$, where "*a*/*b*" denotes the Ce/W molar ratio, such as $Ce_2W_1O_x$, $CeWO_x$ and $Ce_1W_2O_x$. Pristine CeO_x and WO_x were also prepared using the same method as reference samples for activity test and characterizations. The $CeWO_x$ catalyst calcined at 800 ºC for 1 h in air condition was also prepared to investigate its thermal stability for practical use, which was denoted as $CeWO_x$-800. Before the NH_3-SCR activity test, the power catalysts were pressed, crushed and sieved to 40-60 mesh.

In order to comprehensively evaluate the activity of Ce-W mixed oxide catalyst in this study, a conventional V_2O_5-WO_3/TiO_2 catalyst with 4.5 wt.% V_2O_5 and 10

wt.% WO_3 and a Fe-ZSM-5 catalyst with an iron loading of 7 wt.% were prepared as reference materials.

The V_2O_5-WO_3/TiO_2 catalyst with 4.5 wt.% V_2O_5 and 10 wt.% WO_3 was prepared by conventional impregnation method using NH_4VO_3, $(NH_4)_{10}W_{12}O_{41}$, $H_2C_2O_4 \cdot 2H_2O$ as precursors and anatase TiO_2 as support. After impregnation, the excess water was removed in a rotary evaporator at 80 ^oC. The sample was dried at 100 ^oC overnight and then calcined at 550 ^oC for 3h in air condition.

The Fe-ZSM-5 catalyst with an iron loading of 7 wt.% was prepared by incipient wetness impregnation method using $FeCl_2 \cdot 4H_2O$ as precursor and H-ZSM-5 (Si/Al = 25) as support. $FeCl_2 \cdot 4H_2O$ was firstly dissolved in deionized water and then added to H-ZSM-5 to form a paste. The paste was aged for 24 h at room temperature and dried at 60 ^oC overnight. Finally, the sample was calcined in air condition at 550 ^oC for 6 h.

Characterizations

The surface areas of the catalysts were obtained from N_2 adsorption/desorption analysis at 77 K using a Quantachrome Quadrasorb SI-MP. Prior to the N_2 physisorption, the catalysts were degassed at 300 ^oC for 4 h. Surface areas were determined by BET equation in 0.05-0.35 partial pressure range.

Powder X-ray diffraction (XRD) measurements of $Ce_aW_bO_x$ serial catalysts were carried out on a computerized PANalytical X'Pert Pro diffractometer with Cu Kα (λ = 0.15406 nm) radiation. The data of 2θ from 20 to 80 ^{o} were collected at 8 ^{o}/min with the step size of 0.07 ^{o}.

Visible Raman spectra of $Ce_aW_bO_x$ serial catalysts were collected at room temperature on a Spex 1877 D triplemate spectrograph with spectral resolution of 2 cm^{-1}. A 532 nm DPSS diode-pump solid semiconductor laser was used as the excitation source and the power output was about 40 mW. Before measurements, the samples were well ground and mounted into a spinning holder to avoid thermal damage during the scanning. The Raman signals were collected with conventional 90 ^{o} geometry and the time for recording each spectrum was about 1000 ms. All Raman spectra used in the paper were original and unsmoothed.

The XPS of CeO_x, WO_x and $CeWO_x$ were recorded on a Scanning X-ray Microprobe (PHI Quantera, ULVAC-PHI, Inc.) using Al Ka radiation (1486.7 eV). Binding energies of Ce 3d and O 1s were calibrated using C 1s peak (BE = 284.8 eV) as standard.

The *in situ* DRIFTS experiments were performed on an FTIR spectrometer (Nicolet Nexus 670) equipped with a smart collector and an MCT/A detector cooled by liquid nitrogen. The reaction temperature was controlled precisely by an Omega programmable temperature controller. Prior to each experiment, the sample was pretreated at 400 ^{o}C for 0.5 h in a flow of 20 vol.% O_2/N_2 and then cooled down to 200 ^{o}C. The background spectrum was collected in flowing N_2 and automatically subtracted from the sample spectrum. The reaction conditions were controlled as follows: 300 ml/min total flow rate, 500 ppm NH_3, 500 ppm NO, 5 vol.% O_2 and N_2 balance. All spectra were recorded by accumulating 100 scans with a resolution of 4 cm^{-1}.

Influence of H_2O + CO_2 on the SCR activity of $CeWO_x$ catalyst

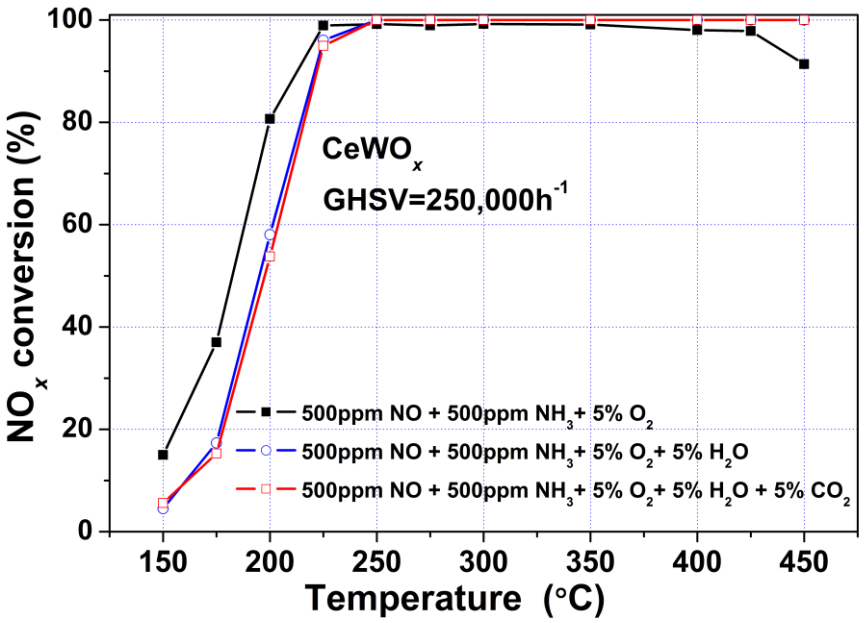

Fig. S1 NH_3-SCR activity of $CeWO_x$ catalyst in the presence of H_2O + CO_2. Reaction conditions: [NO] = [NH_3] = 500 ppm, [O_2] = 5 vol.%, 5 vol.% H_2O, 5 vol.% CO_2, N_2 balance and GHSV = 250,000 h^{-1}.

The description of Fig. S1was already shown in the main text.

BET surface area derived from N_2 physisortion and CeO_2 crystallite size calculated by Scherrer equation from XRD results

Table S1 BET surface area and CeO_2 crystallite size of the catalysts

Sample	BET surface area (m^2/g)	CeO_2 crystallite size (nm)
CeO_x	46.1	17.6
$Ce_2W_1O_x$	44.4	8.8
$CeWO_x$	70.5	9.5
$Ce_1W_2O_x$	74.1	11.8
WO_x	6.1	–

Raman spectra

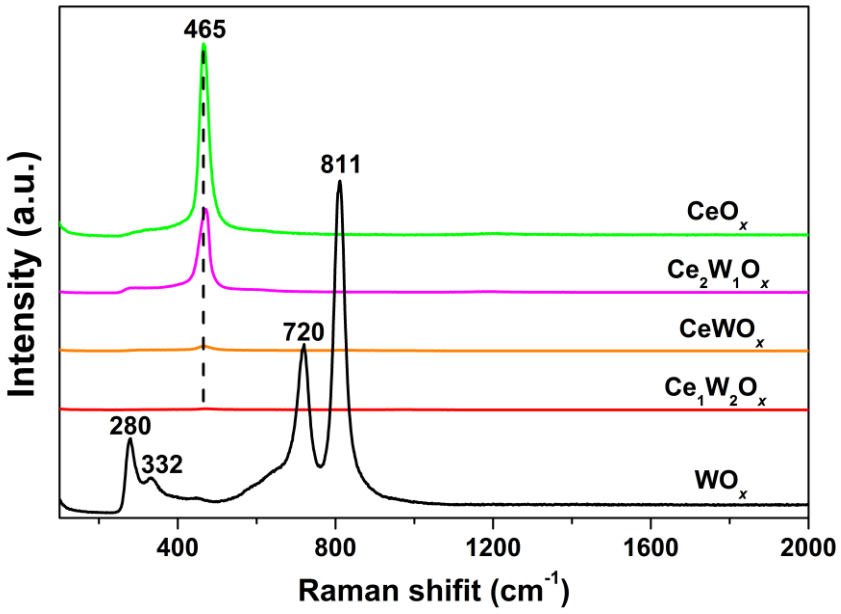

Fig. S2 Raman spectra of $Ce_aW_bO_x$ serial catalysts (λ_{ex} = 532 nm). The peak at 465 cm^{-1} is assigned to CeO_2, and the peaks at 280, 332, 720 and 811 cm^{-1} are assigned to WO_3.

The visible Raman spectra of $Ce_aW_bO_x$ serial catalysts are presented in Fig. S2. The band at 465 cm^{-1} is assigned to the Raman active F_{2g} mode of CeO_2, the typical band of a fluorite structural material.[S1] The bands at 280 and 332 cm^{-1} are assigned to the W-O-W bending modes (F_{2g}) of the bridging oxygen, and the bands at 720 and

811 cm^{-1} are assigned to the W-O stretching mode (A_{1g}) and W-O bending mode (E_g), respectively.[S2-S4] The lower band intensity of CeO_2 on $Ce_aW_bO_x$ serial catalysts showed that the particle size of CeO_2 on the catalyst surface was rather small due to the inhibition of crystallization by W doping. In addition, no WO_3 species was detected at all, which was in well accordance with the XRD results in Fig. 4.

Normalized NH_3-SCR activity by BET surface area

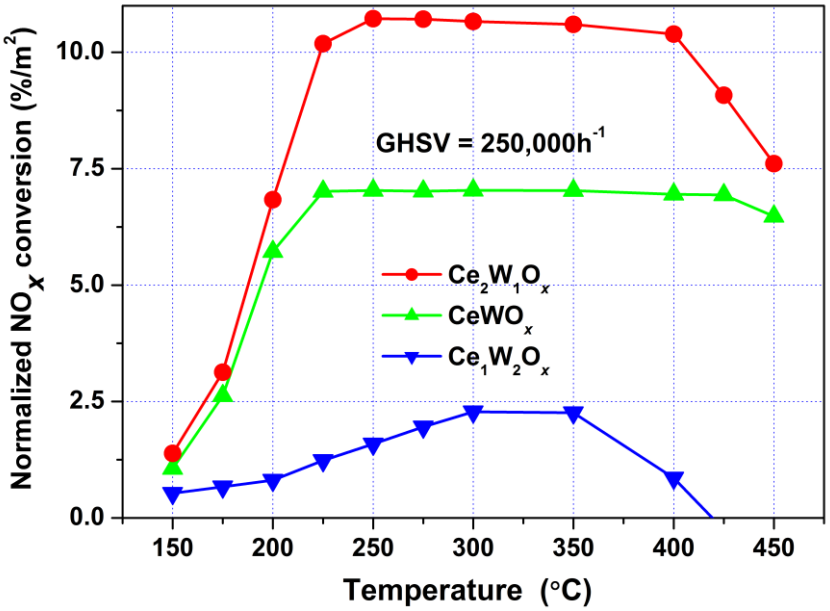

Fig. S3 NH_3-SCR activity of the Ce-W mixed oxide catalysts normalized by BET surface area. Reaction conditions: [NO] = [NH_3] = 500 ppm, [O_2] = 5 vol.%, N_2 balance and GHSV = 250,000 h^{-1}.

In order to deduce the main active component in the Ce-W mixed oxide catalyst, we normalized the NO_x conversion over the catalysts with different Ce/W molar ratios using BET surface area (see Fig. S3). With the increase of Ce/W molar ratio, the normalized NO_x conversion showed a monotonic increase, indicating that small CeO_2 crystallite might be the main active component. Though the normalized NH_3-SCR activity of $CeWO_x$ is lower than that of $Ce_2W_1O_x$, from the viewpoint of application we still chose $CeWO_x$ as the model catalyst for further study due to its high apparent NH_3-SCR activity.

NO and NH_3 oxidation activity

In order to investigate the synergistic effect of Ce and W species in $CeWO_x$ catalyst, the separate NO oxidation (NO + O_2) and separate NH_3 oxidation (NH_3 + O_2) experiments were carried out.

The NO_2 production during separate NO oxidation reaction over CeO_x, WO_x and $CeWO_x$ are shown in Fig. S4. The NO_2 production over $CeWO_x$ is obviously higher than those over pristine CeO_x and WO_x in the low temperature range. Many studies have shown that, if the SCR catalyst can oxidize NO to NO_2 *in situ*, its low temperature SCR activity will be significantly enhanced due to the occurrence of "fast SCR" reaction.[S5,S6] Therefore, the synergistic effect of CeO_x and WO_x could enhance the low temperature activity of $CeWO_x$, by promoting NO oxidation to NO_2 to facilitate the "fast SCR" reaction.

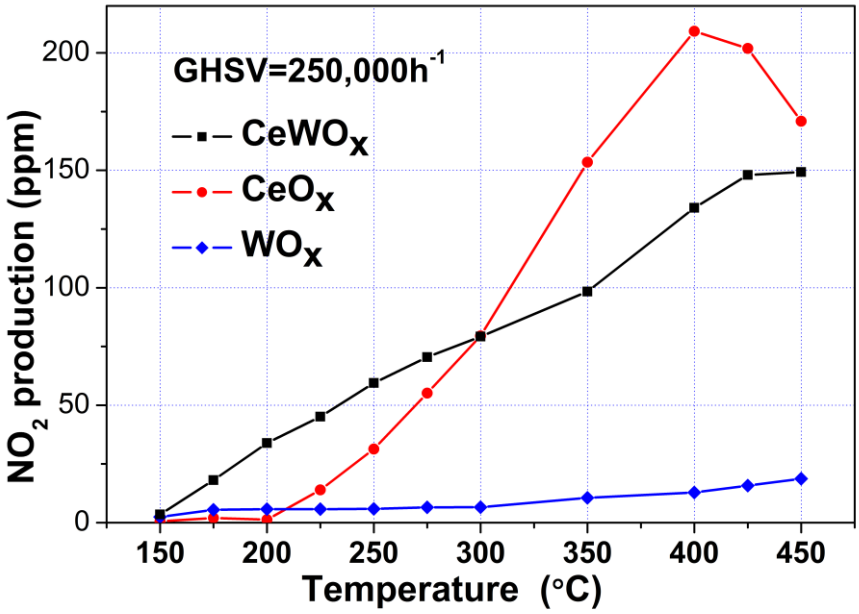

Fig. S4 NO_2 production during separate NO oxidation reaction over CeO_x, WO_x and $CeWO_x$. Reaction conditions: [NO] = 500 ppm, [O_2] = 5 vol.%, N_2 balance and GHSV = 250,000 h^{-1}.

The NH_3 oxidation activities of CeO_x, WO_x and $CeWO_x$ are presented in Fig. S5. The NH_3 oxidation ability of $CeWO_x$ is obviously higher than those of pristine CeO_x and WO_x, which means that synergistic effect of CeO_x and WO_x makes the $CeWO_x$ catalyst more effective in NH_3 activation. Besides, the N_2 selectivity in NH_3 oxidation

reaction over $CeWO_x$ catalyst was much higher than that over CeO_x, suggesting that the introduction of W species into $CeWO_x$ catalyst greatly suppressed the unselective oxidation of NH_3 to N_2O or NO_x, which is also beneficial to the enhancement of N_2 selectivity in NH_3-SCR reaction.

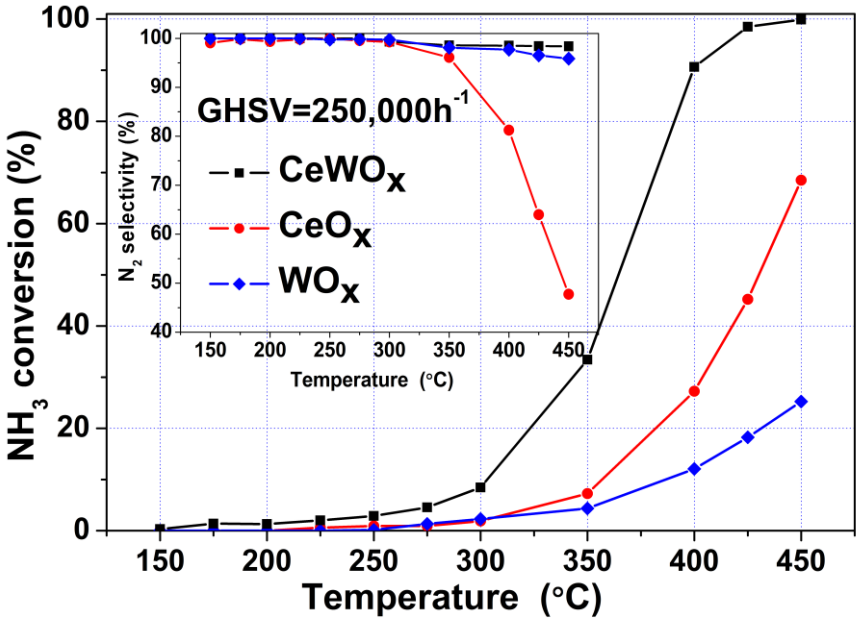

Fig. S5 Separate NH_3 oxidation activity and corresponding N_2 selectivity (inserted) over CeO_x, WO_x and $CeWO_x$. Reaction conditions: $[NH_3]$ = 500 ppm, $[O_2]$ = 5 vol.%, N_2 balance and GHSV = 250,000 h^{-1}.

XPS results

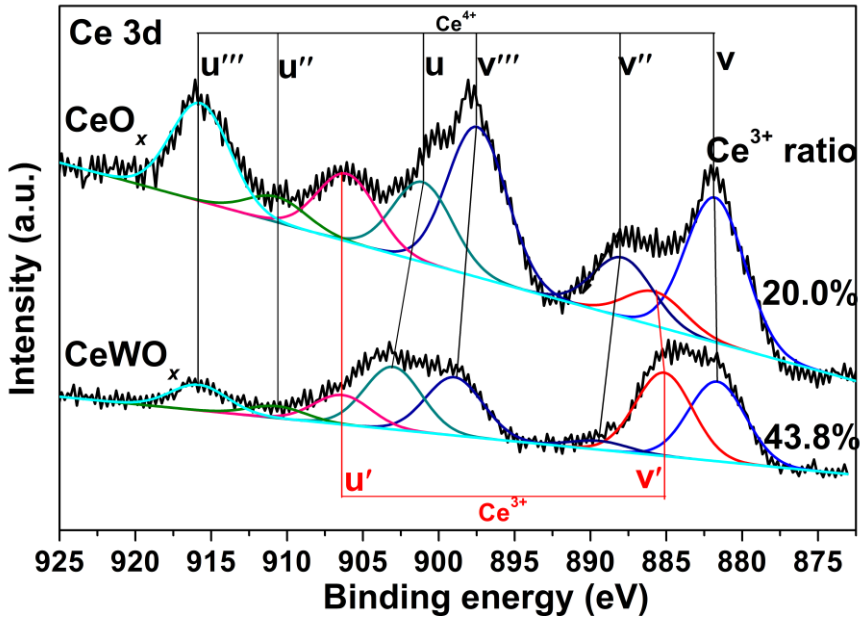

Fig. S6 XPS results of Ce 3d of CeO_x and $CeWO_x$.

The XPS results of Ce 3d on CeO_x and $CeWO_x$ are shown in Fig. S6. The Ce 3d peaks were fitted by searching for the optimum combination of Gaussian bands with the correlation coefficients (r^2) above 0.99. The sub-bands labeled u' and v' represent the $3d^{10}4f^1$ initial electronic state corresponding to Ce^{3+}, and the sub-bands labeled u, u", u"', v, v", and v"' represent the $3d^{10}4f^0$ state of Ce^{4+}.[S7,S8] The Ce^{3+} ratio on $CeWO_x$ (37.2%) calculated by $Ce^{3+}/(Ce^{3+} + Ce^{4+})$ is much higher than that on CeO_x (7.8%). The higher Ce^{3+} ratio in $CeWO_x$ indicates the presence of more surface oxygen vacancies, which will facilitate the adsorption of oxygen species or activate reactants in SCR reaction.

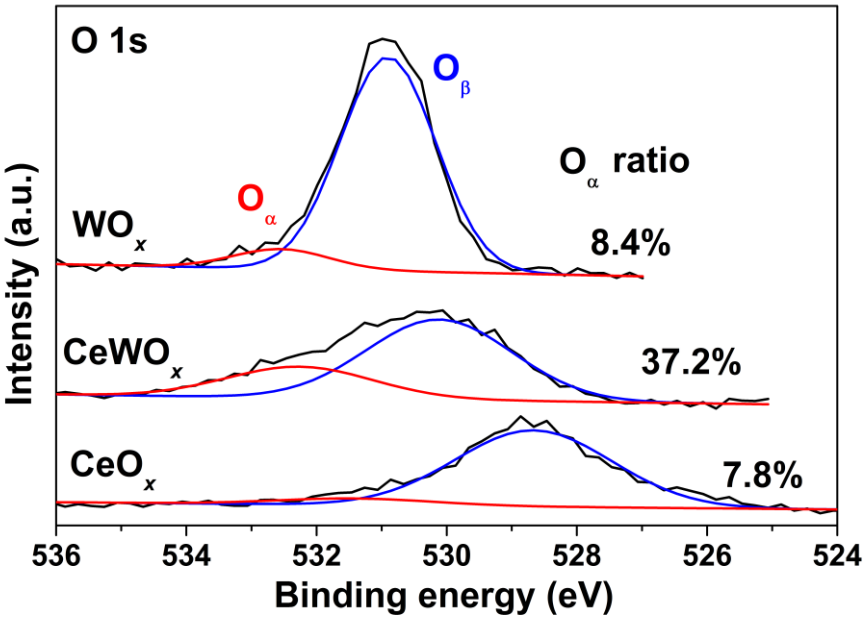

Fig. S7 XPS results of O 1s of CeO_x, WO_x and $CeWO_x$.

The XPS results of O 1s on CeO_x, WO_x and $CeWO_x$ are shown in Fig. S7. The O 1s peak was fitted into two sub-bands by searching for the optimum combination of Gaussian bands with the correlation coefficients (r^2) above 0.99. The sub-bands at lower binding energy (528.7-530.9 eV) corresponded to the lattice oxygen O^{2-} (denoted as O_β), and the sub-bands at higher binding energy (531.4-532.5 eV) corresponded to the surface adsorbed oxygen (denoted as O_α), such as O_2^{2-} or O^- belonging to defect-oxide or hydroxyl-like group.[S9] The O_α ratio on $CeWO_x$ (37.2%) calculated by $O_\alpha/(O_\alpha + O_\beta)$ is much higher than those on CeO_x (7.8%) and WO_x (8.4%), which means that the synergistic effect between Ce and W species indeed resulted in more surface oxygen vacancies. Usually, O_α is more reactive in oxidation

reactions due to its higher mobility than O_β.[S10] Therefore, the higher O_α ratio on $CeWO_x$ is beneficial for the NO oxidation to NO_2 in the SCR reaction and thereafter facilitate the "fast SCR" reaction.

***In situ* DRIFTS study**

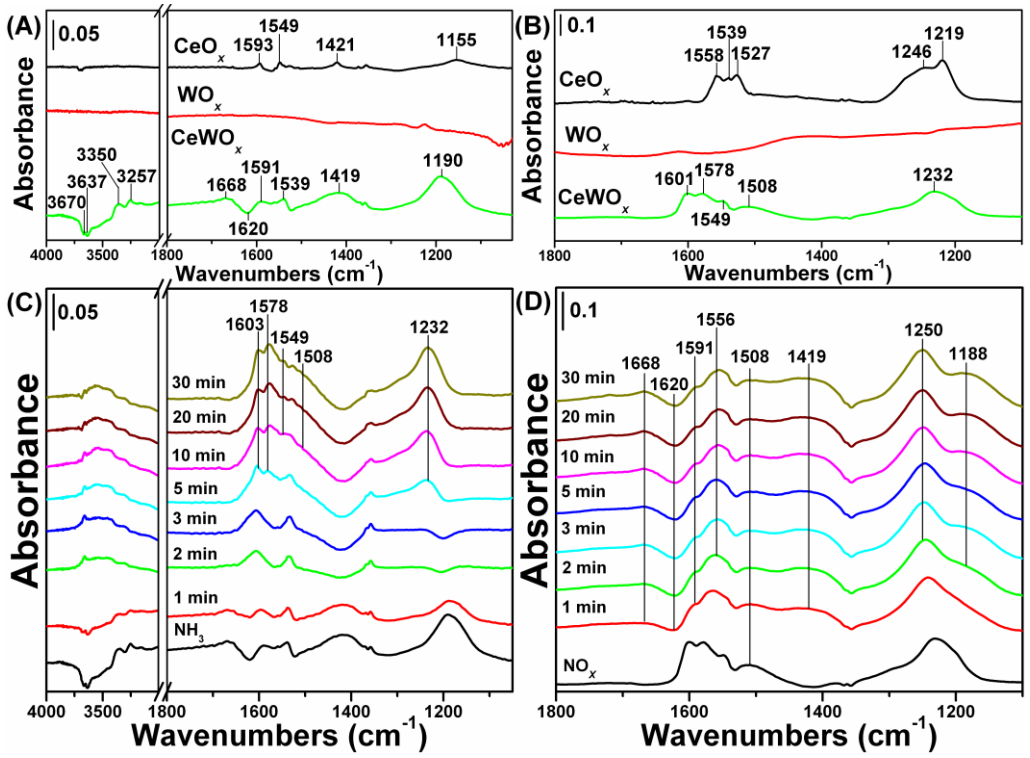

Fig. S8 *In situ* DRIFTS of (A) NH_3 adsorption, (B) NO + O_2 adsorption, (C) NO + O_2 reacted with pre-adsorbed NH_3 species, and (D) NH_3 reacted with pre-adsorbed NO_x species at 200 ^oC on $CeWO_x$ catalyst.

Band assignments:[S9,S11-S18]

(A) 1668 cm^{-1} and 1419/1421 cm^{-1}: symmetric and asymmetric bending vibrations of ionic NH_4^+; 1591/1593 cm^{-1} and 1190/1155 cm^{-1}: asymmetric and symmetric bending vibrations of coordinated NH_3; 1539/1549 cm^{-1}: scissoring vibration mode of NH_2 species; 3257 and 3350 cm^{-1}: N-H stretching vibration modes; 1620 cm^{-1} and 3637, 3670 cm^{-1}: hydroxyl consumption due to the interaction with NH_3 to form NH_4^+.

(B) 1601/1558 cm^{-1} and 1232/1219 cm^{-1}: bridging nitrate; 1578/1539 cm^{-1}: bidentate nitrate; 1549/1527 cm^{-1}: monodentate nitrate; 1508 cm^{-1}: unknown species.

(C) 1603 and 1232 cm^{-1}: bridging nitrate; 1578 cm^{-1}: bidentate nitrate; 1549 cm^{-1}: monodentate nitrate; 1508 cm^{-1}: unknown species.

(D) 1668 and 1419 cm^{-1}: symmetric and asymmetric bending vibrations of ionic NH_4^+; 1591 and 1188 cm^{-1}: asymmetric and symmetric bending vibrations of coordinated NH_3; 1620 cm^{-1}: hydroxyl consumption due to the interaction with NH_3 to form NH_4^+; 1556 cm^{-1}: bidentate nitrate with red shift; 1250 cm^{-1}: surface ammonium nitrate species.

The description of Fig. S8 was already shown in the main text.

References

S1 M. Luo, J. Chen, L. Chen, J. Lu, Z. Feng and C. Li, *Chem. Mater.* 2001, **13**, 197.

S2 S. S. Chan, I. Wachs, L. L. Murrell and N. C. Dispenziere, *J. Catal.*, 1985, **92**, 1.

S3 C. Santato, M. Odziemkowski, M. Ulmann and J. Augustynski, *J. Am. Chem. Soc.* 2001**, 123**, 10639.

S4 A. S. Mamede, E. Payen, P. Grange, G. Poncelet, A. Ion, M. Alifanti and V.I. Pârvulescu. *J. Catal.*, 2004, **223**, 1.

S5 G. Qi and R. T. Yang, *Appl. Catal., B*, 2003, **44**, 217.

S6 F. Liu, H. He, C. Zhang, Z. Feng, L. Zheng, Y. Xie and T. Hu, *Appl. Catal., B*, 2010, **96**, 408.

S7 L. Chen, J. Li and M. Ge, *J. Phys. Chem. C*, 2009, **113**, 21177.

S8 G. Li, D. Zhang and J. C. Yu, *Phys. Chem. Chem. Phys.*, 2009, **11**, 3775.

S9 F. Liu, H. He, Y. Ding, C. Zhang, *Appl. Catal., B*, 2009, **93**, 194.

S10 Z. Wu, R. Jin, Y. Liu and H. Wang, *Catal. Commun.*, 2008, **9**, 2217.

S11 Z. Liu, P.J. Millington, J.E. Bailie, R.R. Rajaram and J.A. Anderson, *Microporous Mesoporous Mater.*, 2007, **104**, 159.

S12 W.S. Kijlstra, D.S. Brands, H.I. Smit, E.K. Poels and A. Bliek, *J. Catal.*, 1997, **171**, 219.

S13 G.M. Underwood, T.M. Miller and V.H. Grassian, *J. Phys. Chem. A*, 1999, **103**, 6184.

S14 W.S. Kijlstra, D.S. Brands, E.K. Poels and A. Bliek, *J. Catal.*, 1997, **171**, 208.

S15 G. Ramis, M.A. Larrubia and G. Busca, *Top. Catal.*, 2000, **11-12**, 161.

S16 G. Busca, M.A. Larrubia, L. Arrighi and G. Ramis, *Catal. Today*, 2005, **107-108**, 139.

S17 L. Lietti, G. Ramis, F. Berti, G. Toledo, D. Robba, G. Busca and P. Forzatti, *Catal. Today*, 1998, **42**, 101.

S18 N.Y. Topsøe, *Science*, 1994, **265**, 1217.